CHARACTERIZATION AND PREDICTION OF AUSTENITE FORMATION AND DECOMPOSITION IN STEEL WELDS

S. S. Babu[1], J. M. Vitek[1], S. A. David[1], T. Palmer[2], J. W. Elmer[2]

[1]Oak Ridge National Laboratory, Oak Ridge, TN 37831
[2]Lawrence Livermore National Laboratory, Livermore, CA 94550

Abstract

Austenite formation and its decomposition control the final microstructure and performance of steel welds. This paper presents an *in-situ* characterization of austenite formation and its decomposition in both the fusion zone (FZ) and heat-affected zone (HAZ) of an Fe-C-Al-Mn steel using time-resolved X-ray diffraction (TRXRD) with synchrotron radiation. Measurement of X-ray diffraction spectra at a time resolution of 0.05 s allowed monitoring of the sequence of phase evolution in welds. In steel containing 1.7 wt.% Al, incomplete austenite formation from the ferrite microstructure was observed in the HAZ during weld heating, which is in agreement with equilibrium thermodynamic predictions. In the case of the FZ, nonequilibrium austenite solidification was observed at high cooling rates, followed by its decomposition during the latter stages of the cooling cycle. A theoretical treatment of both austenite formation and its decomposition in these welds, based on existing thermodynamic and kinetic models is used to explain these experimental results.

Introduction

Austenite formation and decomposition in both the weld heat-affected-zone (HAZ) and the weld fusion zone (FZ) is a well-studied phenomenon in the welding metallurgy of steels [1]. In the HAZ, the room temperature microstructure transforms to 100 % austenite on heating above the Ac_3 temperature. This transformation may or may not reach completion depending upon the peak temperature (between Ac_1 and Ac_3) attained in the HAZ and the time over which the material experiences this temperature. Interestingly, the temperature near the fusion line may be high enough to form the high temperature δ-ferrite phase.

The austenite and δ-ferrite phases that form in the FZ and HAZ during heating will transform to several different low-temperature phases during cooling. For example, the δ-ferrite in the HAZ may transform back to austenite, which may then transform to different morphologies of α-ferrite, namely, allotriomorphic ferrite, Widmantstätten ferrite, and bainite. At rapid cooling rates, the austenite will transform to martensite. In the fusion zone during cooling, the liquid solidifies as δ-ferrite, which then transforms to austenite. With continued cooling, the austenite transforms to the different α-ferrite morphologies observed in the HAZ microstructure.

Due to the steep temperature gradients and dynamic cooling conditions of welds, the resulting material contains significant microstructural gradients. These microstructural gradients affect the strength, ductility, toughness, fatigue and creep rupture properties of steel welds. The knowledge of these gradients is well developed and is routinely considered in the design of weldments. However, there is a need to develop predictive models to describe these gradients as a function of steel composition and weld thermal cycles. Previously published experimental work has investigated the phase evolution in the HAZ and FZ of a Fe-C-Al-Mn steel weld using

in-situ measurements [2]. In this investigation, the measured phase evolution is interpreted using computational thermodynamic and diffusion controlled growth models.

Experimental

Material and Welding

The welds were made by striking an arc on a stationary steel cylinder of 10.16-cm diameter. The steel cylinder composition was Fe – 0.234C – 0.50 Mn – 1.70 Al – 0.28 Si – 0.02 Ni – 0.003 Ti – 0.006 O – 0.064 N (wt.%). These cylinders were mounted on a fixture that was placed inside a chamber with a porthole allowing for X-ray entrance. Spot welds were produced on these bars to melt and resolidify the steel using the gas-tungsten arc-welding process. The average welding power was maintained constant at 1.9 kW (110 A, 17.5 V), and current pulsing was used to help minimize the side-to-side motion of the liquid weld pool. Helium was used as the welding and shielding gas, and a cross jet of helium was used to blow the evaporated metal powders away from the area where the X-ray diffraction measurements were being made. In this experiment, the arc was extinguished at 17 s after initiation. This leads to slow heating conditions in the HAZ and rapid cooling conditions in the fusion zone region [3]. During this experiment, the phase transformation events in both the HAZ and the FZ were monitored using the Time Resolved X-Ray Diffraction (TRXRD) technique.

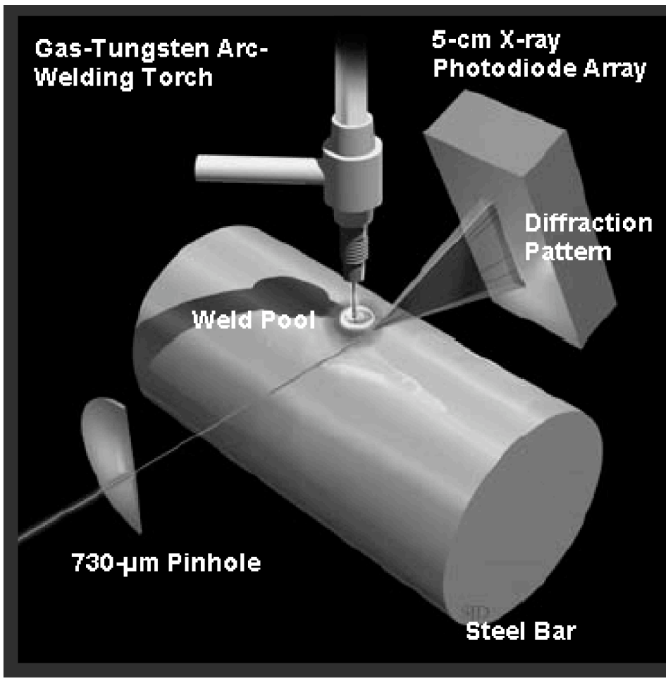

Fig. 1 Schematic illustration of the X-ray diffraction and welding set up used in the present research

Time Resolved X-ray Diffraction

TRXRD measurements were performed on a 31-pole wiggler 10-2 beam line [4] at Stanford Synchrotron Radiation Laboratory with the Stanford Positron Electron Accumulation Ring operating at an electron energy of 3.0 GeV and an injection current of ~ 100 mA. A 730-□m-diameter pinhole was used, yielding a beam flux on the sample of 10^{10} to 10^{11} photons/s, as determined experimentally using an ion chamber downstream from the pinhole. A photon energy of 12.0 keV (□= 0.1033 nm) was chosen to maximize the number of peaks diffracting into the 2□ window of the X-ray detector. The diffraction intensities at various 2□ positions were monitored continuously and in real

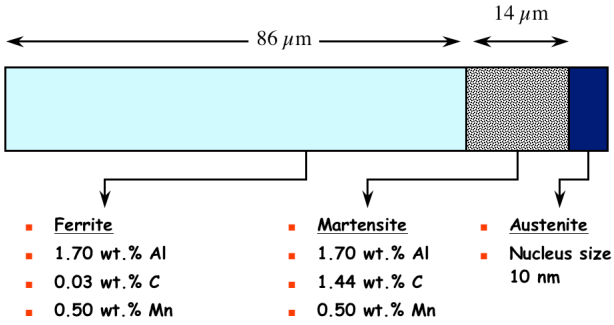

Fig. 2 Schematic illustration of the simulation geometry and boundary conditions used in diffusion controlled calculation of austenite formation and growth in the HAZ of the weld

time using a 5 cm-long photodiode array covering a 2θ range of approximately 30°. The diffraction spectra were collected at 0.05-s time intervals during transient heating and cooling of spot welds. An overview of the experimental setup is shown in Fig. 1.

Thermodynamic and Kinetic calculations

The equilibrium thermodynamic phase evolution was predicted using ThermoCalc® software [5] version N with the solid solution database. The calculations considered equilibrium between liquid, ferrite (bcc), austenite (fcc) and cementite (Fe_3C). In addition to equilibrium thermodynamic calculations, the diffusion controlled growth of austenite to ferrite during the weld heating was simulated using DicTra® software [6]. In these calculations, solid solution thermodynamic- and standard mobility-databases were used. The geometry used for the simulation is shown in Fig. 2. In this case, the room temperature microstructure is taken as a mixture of ferrite and 14% martensite based on optical microscopy analysis. The carbon concentration of ferrite was fixed at 0.03 wt.%, based on thermodynamic calculations at 800 K. The carbon concentration of martensite was fixed based on nominal composition and ferrite fraction. The simulations were performed with two assumed heating rates of 495 × time$^{0.25}$ and 395 × time$^{0.25}$ from 800 K. These heating rates are similar to the results presented by Zhang et al [3] for C-Mn steel spot welds. These simulations were not continued for the microstructural evolution during cooling cycle due to the inability to consider departure from local equilibrium conditions at the interface.

The phase evolution of the FZ during solidification was predicted using published interface response function models [7] that predict the solid-liquid interface temperature and dendrite growth morphologies [2]. For multicomponent alloy dendrite solidification, there are equations describing the velocity-dependent parameters, including the partitioning coefficient (k_V^i), liquidus slope (m_V^i), dendrite tip radius (R), dendrite tip liquid concentration (c_l^{i*}) and dendrite/cellular tip temperature ($T_{d/c}$), which are given by Eqs. (1), (2), (3), (4), and (5), respectively.

$$k_V^i = k_o^i + a_o\left(V_s/D_i\right)\Big/\left[1 + a_o\left(V_s/D_i\right)\right] \tag{1}$$

In Eq. (1), k_o^i is the equilibrium partition coefficient for each alloying element "i" in liquid/solid boundary, a_o is the characteristic diffusion distance, D_i is the solute diffusivity at the liquid solid boundary for element "i", and V_s is the solid-liquid interface velocity.

$$m_V^i = m_o^i\left(1 - k_V^i\left(1 - \ln\left\{k_V^i/k_o^i\right\}\right)\Big/1 - k_o^i\right) \tag{2}$$

In Eq. (2), m_o^i is the equilibrium liquidus slope of i^{th} element. The radius of the dendrite tip is calculated by solving the following equation.

$$4\Gamma^2\left(1/R^2\right) + \left(2\sum_i\left[m_V^i Pe^i\left(1 - k_V^i\right)c_l^{i*}\Delta_C^i\right]\right)\left(1/R\right) + G = 0 \tag{3}$$

In Eq. (3), Γ is the Gibbs-Thompson coefficient and Pe^i is the Peclet number for each alloying element given by the relation $Pe^i = V_s R/2D_i$. In the present work, the boundary diffusivity (D_i) was assumed identical for all the alloying elements. Therefore, the Pe^i is the same for all alloying elements. The parameter Δ_C^i is a function of the solute Peclet number as given in [8]. The parameter G in Eq. (3) is the temperature gradient.

$$c_l^{i*} = c_o^i\Big/\left[1 - \left(1 - k_V^i\right)Iv\left\{Pe^i\right\}\right] \tag{4}$$

In Eq. (4), c_l^{i*} is the liquid concentration for alloying elements at the interface, "*i*", and $Iv\{Pe^i\}$ is the Ivantsov function that depends on the Peclet number. The value of $Iv\{Pe^i\}$ as a function of the Peclet number is given in reference 8. It is important to note that $Iv\{Pe^i\}$ is also related to the effective supersaturation, Ω, given by $Iv\{Pe^i\} = \Omega_i = (c_l^{i*} - c_o^i)/(c_l^{i*} - c_s^{i*})$. In this relation, c_s^{i*} is the dendrite tip solid concentration of the i^{th} alloying element and c_o^i is the nominal concentration of "*i*" in the bulk alloy.

$$T_{d/c} = T_l + \sum_i \left(c_l^{i*} m_V^i - c_o^i m_o^i\right) - 2\Gamma/R - V_s/\mu - GD/V_s \qquad (5)$$

In Eq. (5), T_l is the equilibrium liquidus temperature of the initial alloy composition and μ is the interface kinetic coefficient. In the present work, the equilibrium liquidus temperature (T_l), slope (m_o^i), and partition coefficient (k_o^i) at T_l were calculated as a function of steel composition using ThermoCalc® software version N [5]. The growth temperature of a single-phase planar front (T_{planar}) is given by Eq. (6). In the planar solidification mode, the solid concentration is the nominal composition of the bulk alloy, and the liquid concentration at the liquid/solid interface is estimated by the velocity-dependent partition coefficient.

$$T_{planar} = T_s + \sum_i c_{o,i}\left(m_V^i / k_V^i - m_o^i / k_o^i\right) - V_s/\mu \qquad (6)$$

In Eq. (6), T_S is the solidus temperature for the initial alloy. Equations (1) through (6) were solved iteratively using numerical techniques. Solutions to these equations 1 to 5 must lead to a unique dendrite tip temperature, concentration, and radius for a given interface velocity for both austenite and ferrite modes of solidification. The equation (6) gives the estimate of the planar interface temperature. If the ferrite tip temperature (either $T_{d/c}$ or T_{planar}) is higher than that of austenite, one can conclude that the ferrite mode of solidification prevails for a given velocity. For details, the reader is referred to prior published works [2]. In this research, the primary mode of solidification was calculated using these models and compared with the TRXRD observations.

Results

The macrostructure of the spot weld is shown in Fig. 3. TRXRD measurements were made in both the HAZ and the FZ regions of the spot weld. It is noteworthy that due to the small penetration of the x-rays, the measurements are relevant to only the surface of the welds. Due to the steep temperature gradients, the TRXRD measurements from the HAZ correspond to regions with different peak temperatures that vary by as much as 50K across the diameter of the X-ray beam.

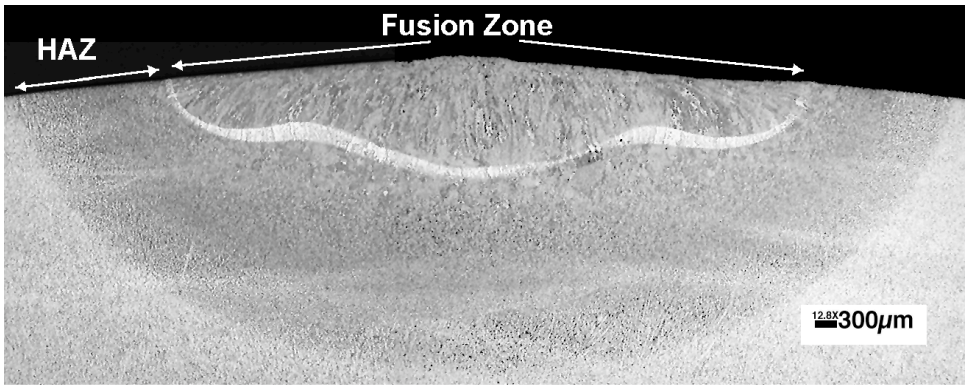

Fig. 3 Macrostructure of the spot weld made during TRXRD measurements. The HAZ and FZ zone regions are marked. The TRXRD measurements were made on the surface.

Phase Evolution in the Heat Affected Zone

The measured TRXRD data from a location in the HAZ (very close to the fusion zone boundary) are shown in Fig. 4*a* in the image format, for a 2θ region of 28º to 30º. The black lines show the diffraction peak locations and the intensity is represented by the darkness of these lines. Before the initiation of the arc, diffraction from only the bcc phase (ferrite) was observed at room temperature. As soon as the arc was initiated, the diffraction lines from ferrite shifted toward lower 2θ values, indicating the expansion of the bcc lattice. After 6 s, the fcc diffraction peaks appeared, indicating the formation of austenite. With continued heating, the peak intensity of austenite increased, indicating that the austenite fraction is increasing as well. Interestingly, the results show that over the course of the heating, the ferrite to austenite transformation does not reach completion. When the arc was extinguished (17 s), the austenite rapidly transformed to ferrite/martensite. Due to the experimental set up, the observed bcc peaks could not be delineated from bcc (ferrite) or body centered tetragonal (bct) martensite structure. However, the optical microscopy did reveal the formation of both bainite and martensite [see Fig. 4*b*].

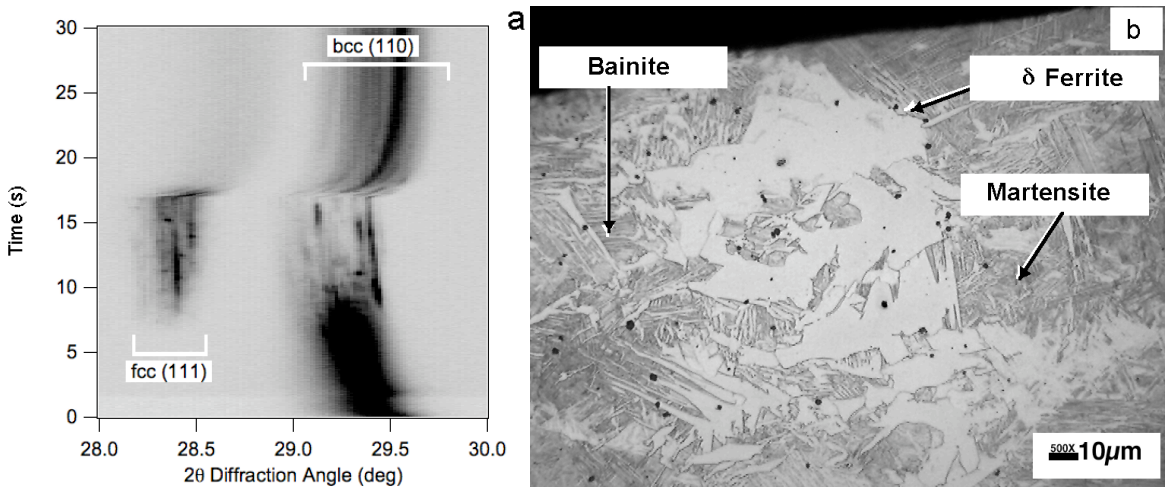

Fig. 4 (*a*) TRXRD results from the HAZ of the weld. The dark contrast corresponds to intensity of the diffraction lines. (*b*) Microstructure of the HAZ showing the presence of coarse δ-ferrite and bainite and martensite that formed from the austenite.

Phase Evolution in Fusion Zone

The measured TRXRD data from a location in the FZ (~4 mm from the center of the weld) are shown in Fig. 5*a* in the image format. The measurements were started after the arc-initiation, at which time, only liquid is present at the measurement location. This is confirmed by the absence of any diffraction information for the first 2 seconds of the TRXRD plot in Fig. 5*a*. As soon as the arc was extinguished, the TRXRD measurements, in direct contradiction to previous research on these steels [9], showed the formation of austenite. The fcc diffraction lines shifted towards higher 2θ values during the initial stages of cooling, indicating that the lattice is contracting. On continued cooling, the austenite transforms to a ferrite/martensite mixture with the reduction of austenite peak intensity and the appearance of the bcc peak.

Similar to the HAZ results, it is difficult to distinguish ferrite from martensite in these diffraction peaks. Calculated 2θ separation of (011) and (110) martensite diffraction peaks are expected to be in the order of 0.4° for the bulk carbon concentration. However, due to the spread of the peaks due to experimental diffraction geometry makes the delineation of martensite and ferrite peaks difficult. Careful analysis showed a slow increase in bcc diffraction at high temperature and a rapid increase at low temperature, suggesting that the microstructure may have both ferrite and martensite in the microstructure. The optical

microscopy confirmed the predominant presence of bainite and martensite (Fig. 5*b*). Although, the optical microscopy revealed some allotriomorphic ferrite, it is difficult to identify positively whether this ferrite formed during the solid-state transformation of austenite or during solidification in the interdendritic regions of austenite.

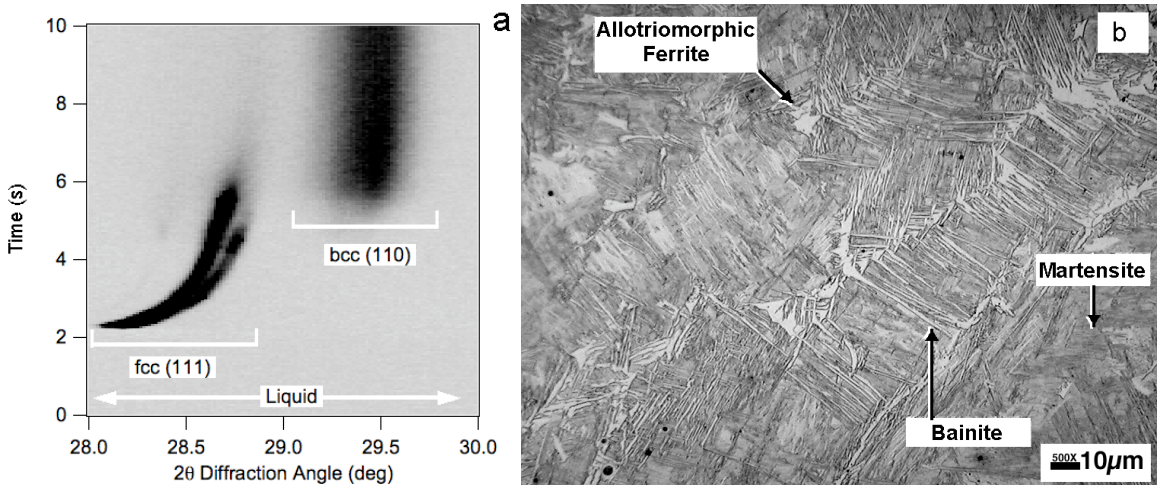

Fig. 5 (*a*) TRXRD results from the FZ of the weld. The dark contrast corresponds to intensity of the diffraction lines. (*b*) Microstructure of the FZ showing the presence of allotriomorphic ferrite, bainite and martensite that formed from austenite during cooling.

Discussions

The TRXRD and optical microscopy results together showed two interesting phenomena. First, in the HAZ region, the ferrite that is present at room temperature was never completely replaced by austenite, i.e., austenite formation was incomplete. It is stressed that under the welding conditions used in the present work, the HAZ experiences a rather slow heating rate, during 17 s of welding arc time. In contrast, it experiences rapid cooling from high temperatures after arc-extinction. Second, in the FZ region, the liquid solidified as austenite instead of the expected □-ferrite. Similar to the HAZ, the FZ region experiences a slow heating rate up to the melting point. However, on heating above the melting point, previously existing microstructure is destroyed. After arc-extinction, the FZ region experiences a much more rapid cooling cycle than the HAZ. In this section, attempts are made to model these phenomena using computational thermodynamic and kinetic models.

Prediction of austenite formation in the HAZ during heating

Thermodynamic calculations showed that the steel used in this research would never transform to 100% austenite on heating [see Fig. 6*a*]. This is in contrast to a simple Fe-C-Mn steel, in which the room temperature ferrite - pearlite microstructure transforms to 100% austenite [10]. This observation of incomplete austenite formation is in qualitative agreement with the experimental data shown in Fig. 4*a*. This TRXRD data is converted into an estimated volume fraction of ferrite using a peak area analysis [11]. The measured results are compared with the predicted ferrite fraction for two heating cycles in Fig. 6*b*. The kinetics of austenite formation was predicted by using diffusion controlled growth models for the conditions described earlier. The experimental data show a reduction of ferrite to 30%, while the predicted ferrite fraction reduced to 46% with a peak temperature of 1502 K and to 47% with a peak temperature of 1680 K. The calculations with a peak temperature of 1680 K show reduction of ferrite initially and growth above a critical temperature. This is related to higher stability of ferrite at these temperatures.

The trends observed in the experiments generally agree with the predictions, except with the reduction of ferrite to 30%. This is attributed to the temperature gradient within the measurement volume in the HAZ, as well as, the simplistic geometry and heating cycle used in the simulation. It is important to note that these simulations were aimed at evaluating the applicability of the diffusion controlled growth models for a given thermal cycle and further work is needed to understand the spatial variation of peak temperatures, rate of heating, and the change of transformation mode from diffusion controlled to possible massive transformation of ferrite to austenite.

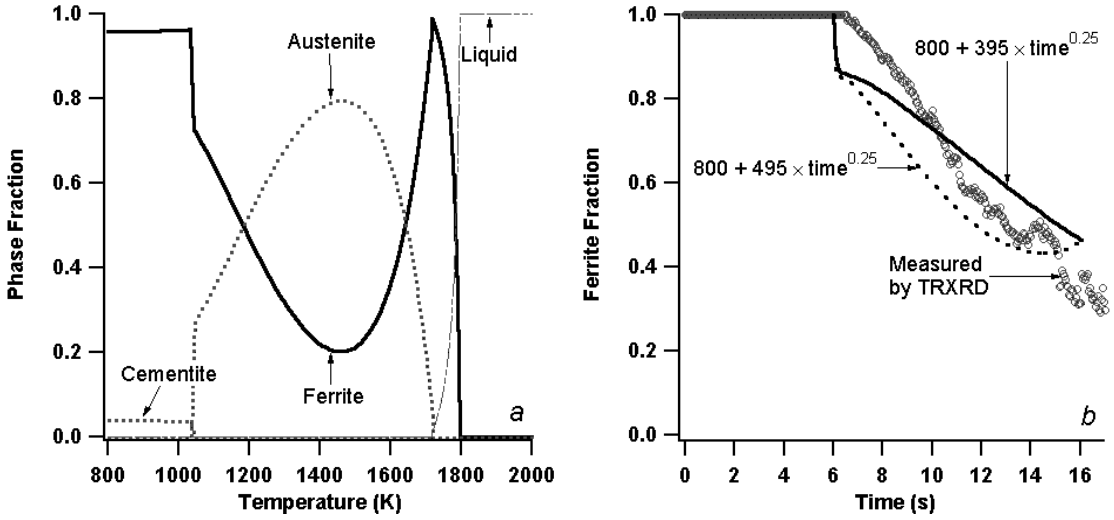

Fig. 6 (*a*) Predicted equilibrium phase fraction as a function of temperature shows that 100%austenite formation is impossible in this alloy. (*b*) Measured ferrite fraction is compared with predicted ferrite fraction for two thermal cycles (with instantaneous heating to 800 K at 6 seconds).

Phase Evolution in FZ

The calculated ferrite fractions given in Fig. 6a show that the primary solidification in these alloys should be δ-ferrite. In agreement with predictions, the welds under normal cooling conditions exhibit columnar δ-ferrite microstructure [12]. On the other hand, the TRXRD results from the FZ indicated primary austenite solidification. This transition from δ-ferrite to austenite solidification is attributed to a rapid increase in the liquid-solid interface velocity brought about by the high cooling rate experienced during the TRXRD experiments. Previous work showed that by reducing the cooling rate in these spot welds, the equilibrium δ-ferrite solidification could be observed [2].

Similar changes in solidification mode from ferrite to austenite have been observed in rapidly cooled stainless steel welds [7], as determined by post-weld characterization. However, in the current alloy, such changes cannot be inferred from post-weld microstructures due to the destruction of the solidification microstructure by solid-state transformations. The observation of bainitic ferrite and martensite in the fusion zone at room temperature [see Fig. 5*b*] does not present any clues about solidification microstructure. The results from optical microscopy alone are ambiguous, giving two possible mechanisms for the evolution of the microstructure:

Liquid → *δ ferrite* → *austenite by massive transformation* → *bainite + martensite* (7)

Liquid → *austenite by nonequilibrium solidification* → *bainite + martensite* (8)

The TRXRD results showed that in these welds sequence II is the operating mechanism, whereby the weld solidifies directly to the non-equilibrium austenite phase before transforming to bainite and martensite.

Such phase selection in weld solidification can be evaluated using interface-response function models. These models have been successfully applied to predict the non-equilibrium austenite formation in stainless steel welds [7]. Using this model, the liquid-δ-ferrite interface and liquid - austenite interface temperatures can be estimated as a function of interface velocity. If the temperature of the liquid-δ-ferrite interface is higher than that of the liquid - austenite interface, one can conclude that the liquid-δ-ferrite will lie ahead of the liquid - austenite interface. In other words, this will suggest primary mode of solidification by δ-ferrite. The opposite will be true for the primary mode of solidification by austenite. The same methodology was extended to the present steel.

Thermodynamic parameters for the model were calculated using ThermoCalc® software. The results based on the published Gibbs - Thompson coefficient Γ for stainless steels are shown in Fig. 7*a*. The results show that the liquid – δ-ferrite interface temperatures for both dendritic and planar mode of solidification are always higher than that of the liquid – austenite interface. The expected velocity ranges for the present welding conditions [2] are also shown in Fig. 7*a*. The calculations show that the transition to the austenite mode of solidification is not expected. This prediction is contrary to the experimental observation. Additional calculations were made to assess the sensitivity of the results to the Gibbs - Thompson coefficient, Γ. By arbitrarily changing the value of Γ for ferrite from 2.6 X 10^{-7} to 2.6 X 10^{-6}, the interface temperature could be reduced to a temperature below that of austenite. With these new calculations [see Fig. 7*b*], the austenite dendrite-tip interface would lie ahead of the ferrite dendrite-tip interface, resulting in an austenitic mode of solidification. This is in agreement with experimental observations. Furthermore, at lower velocities, the δ-ferrite solidification would prevail, as found experimentally in slow cooled spot welds [2].

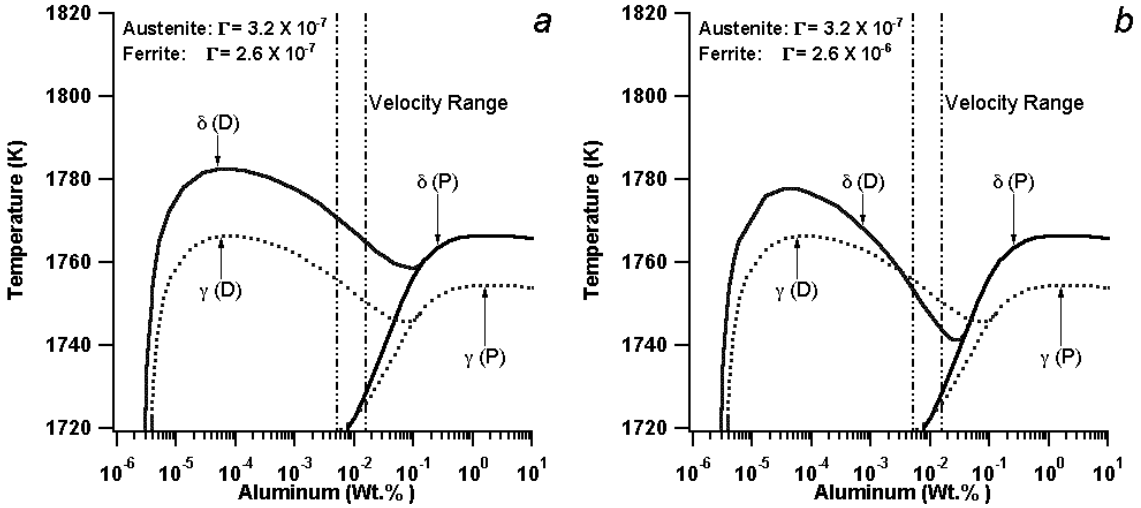

Fig. 7 (*a*) Predicted liquid-δ-ferrite and liquid-γ-austenite interface temperature for both dendritic (D) and planar (P) growth as a function of interface velocity (*a*) with standard Γ Gibbs-Thompson coefficient for both phases and (*b*) with modified Γ value for δ-ferrite.

Although, this is in agreement with experimental measurement, future work is needed to rationalize the selection of an appropriate Gibbs – Thompson coefficient (Γ). The value of Γ is related to the ratio of interfacial energy (σ) and the entropy change (ΔS_f) on melting per unit volume [13, 14]. This suggests that the Γ of liquid-δ-ferrite interface must be higher than that

of liquid-δ-austenite interface during rapid cooling conditions. Arnold et al [14] addressed the calculation of σ based on the model of Spaepen [15]. Spaepen's model relates the σ to ΔS_f and type of crystal structure for monoatomic system. However, these models do not consider the effect of solute trapping on the interfacial energy. Carbon trapping may therefore play an important role in the ferrite solidification. Further work is underway to derive these values as a function of a velocity dependent partitioning coefficient.

Summary and Conclusions

The phase evolution in the HAZ and FZ regions of an Fe-C-Al-Mn steel weld was characterized using Time-Resolved X-ray Diffraction. The results from the HAZ region showed that the ferrite phase was partially stable and do not revert to 100% austenite on heating, which is in agreement with thermodynamic calculations. The diffusion controlled growth model calculations showed that the reduction in ferrite by the austenite growth was closely related to the peak temperatures achieved during the weld thermal cycle. TRXRD results from the rapidly cooled fusion zone indicated the formation of non-equilibrium austenite, contrary to the equilibrium δ-ferrite that was observed under normal weld cooling conditions. Interface response function models with published thermodynamic parameters showed that primary austenite solidification is not expected and that ferrite primary solidification should occur. An analysis of the model showed that the predictions are very sensitive to the assumed Gibbs Thompson interface coefficient. Adjustments in this parameter lead to predictions in agreement with the experimental observations.

Acknowledgement

This research was sponsored by the U.S. Department of Energy, Division of Materials Sciences and Engineering under contract No. DE-AC05-00OR22725 with UT-Battelle, LLC. A portion of this work was performed under the auspices of the U. S. Department of Energy, Lawrence Livermore National Laboratory, under Contract No. W-7405-ENG-48. The authors would like to thank Dr. Joe Wang of LLNL for help with the synchrotron diffraction experiments, Ms. M. A. Quintana of Lincoln Electric, Cleveland, Ohio for providing welds, and Mr. W. Zhang and Prof. T. DebRoy of Pennsylvania State University for allowing us to use the unpublished results of heat- and mass-transfer calculations for gas-tungsten arc spot-welds. The authors thank Drs. J-W. Park and M. Murugananth of ORNL for helpful comments on the manuscript.

References

1. K. E. Easterling, "Introduction to the physical metallurgy of welding," Butterworths, London, 1983.

2. S. S. Babu, J. W. Elmer, J. M. Vitek, and S. A. David, "Time-resolved X-ray diffraction investigation of primary weld solidification in Fe-C-Al-Mn steel welds" *Acta Materialia*, 2002, **50**, 4763-4781.

3. W. Zhang, G. G. Roy, J. W. Elmer and T. DebRoy, "Modeling of heat transfer and fluid flow during gas tungsten arc spot welding of low carbon steel," *J. Applied Physics*, 2003, **93**, 3022-3033.

4. V. Karpenko, J. H. Kinney, S. Kulkarni, K. Neufel, C. Pope, K. G. Tirsell, J. Wong, J. Cernio, T. Troxel, and J. Yang, "Beamline-10 - a multipole wiggler beamline at SSRL," *Review of Scientific Instruments*, 1989, **60**, 1451.

5 B. Sundman, B. Jansson, and J. O. Andersson, "The thermo-calc databank system," *Calphad*, 1985, **9**, 1-153.

6. A. Borgenstam, A. Engstrom, L. Hoglund, J. Agren, "DICTRA, a tool for simulation of diffusional transformations in alloys," *J. Phase Equilibria*, 2000, **21**, 269-280.

7. S. Fukumoto and W. Kurz, "Prediction of the delta to gamma transition in austenitic stainless steels during laser treatment," *ISIJ International*, 1998, **38**, 71-77.

8. W. Kurz and D. J. Fisher, Fundamentals of Solidification, Fourth Revised Edition, Trans Tech Publications Ltd, USA, 1998, Page 242.

9. M. A. Quintana, J. McLane, S. S. Babu, S. A. David, "Inclusion formation in self shielded flux-cored arc welds," *Welding Journal*, 2001, **80**, 98s-105s.

10. J. W. Elmer, T. A. Palmer, W. Zhang, B. Wood, and T. DebRoy, "Kinetic Modeling of Phase Transformations Occurring in the HAZ of C-Mn Steel Welds Based on Direct Observations," in press *Acta Materialia*, January, 2003.

11. T. A. Palmer, J. W. Elmer, and Joe Wong, "In-Situ Observations of Ferrite/Austenite Transformations in Duplex Stainless Steel Weldments Using Synchrotron Radiation," *Science and Technology of Welding and Joining*, Vol. 7(3), pp 159-171, 2002.

12. S. S. Babu, S. A. David, and M. A. Quintana, "Modeling microstructure evolution in self-shielded flux cored arc welds," *Welding Journal*, 2001, **80**, 91s-97s.

13. R. Trivedi and W. Kurz, "Dendritic Growth," *International Materials Reviews,* 1994, **39**, 49-74.

14. C. B. Arnold, M. J. Aziz, M. Schwarz, and D. M. Herlach, "Parameter-free test of alloy dendrite-growth theory," *Physical Review B*, 1999, **59**, 334-343.

15. F. Spaepen, "A structural model for the solid-liquid interface in monoatomic systems," *Acta Metallurgica*, 1975, **23**, 729-743.